

Reaction dynamics of $\text{Na}^*(4^2P) + \text{H}_2$: Effect of reactant orbital alignment on reactivity and product rotational state distribution

Solomon Bililign and P. D. Kleiber

Department of Physics and Astronomy, The University of Iowa, Iowa City, Iowa 52242-1479

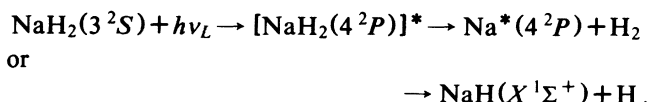
(Received 21 May 1990)

We have investigated the direct reaction of $\text{Na}^*(4^2P)$ with H_2 to form the product NaH . Using far-wing absorption techniques, we have measured absorption into the NaH_2 collision complex, followed by branching into nonreactive (formation of Na^*) or reactive (formation of $\text{NaH}[X^1\Sigma^+(v'',J'')]$) channels. We have observed the reaction to occur both via the attractive potential-energy surfaces and over a barrier on the repulsive surfaces. We have studied the effect of reactant orbital alignment on product rotational distribution for $v''=1$. Specifically we find reaction on the repulsive surfaces leads preferentially to low rotational product states of NaH , while reaction on the attractive surfaces leads preferentially to high rotational states.

Because of their relative simplicity, alkali-metal-hydrogen reactions are theoretically tractable and therefore useful for testing molecular-dynamics models. Despite this simplicity, the reaction dynamics are not well understood.¹⁻³ One approach for investigating these excited-state collisional interactions is to study the far-wing absorption profiles of collision broadened spectral lines.⁴ In the Born-Oppenheimer Franck-Condon limit, absorption in the far wings occurs at a fixed internuclear separation between well-defined molecular electronic states of the collision complex. Far-wing absorption profiles are thus sensitive to the detailed shape of the intermolecular potential-energy surfaces. Measurement of the product rotational and vibrational state distribution following far-wing excitation of the reaction complex provides information about the dynamical evolution in the excited state from the point of absorption into the asymptotic exit channel. For example, far-wing absorption can be used to excite specific molecular electronic symmetry states in the entrance channel and to observe the subsequent reaction probability and final-state branching. The effect of the reactant orbital alignment on the reaction dynamics can provide insight into both the nuclear motion dynamics and nonadiabatic couplings in the process.⁴

We have recently applied this technique to the investigation of the excited-state reaction of $\text{Na} + \text{H}_2$. Here we report on our observations of the direct reaction of $\text{Na}^*(4^2P) + \text{H}_2$ to form NaH . The principle of the experiment is to directly excite the Na-H_2 collision complex from the ground potential surface to an excited-state potential surface which correlates with the $\text{Na}^*(4^2P) + \text{H}_2$ asymptote. This is accomplished by tuning the laser into the far wings of the $\text{Na}(3^2S-4^2P)$ second resonance transition near 330 nm.

The process can be written schematically,



The pseudopotential curves of Rossi and Pascale (Fig. 1) give insight into the far-wing absorption process.⁵ As

the laser is tuned into the far blue wing of the atomic resonance we selectively pump the repulsive potential-energy surface (e.g., 2A_1 in C_{2v} geometry or $^2\Sigma^+$ in $C_{\infty v}$ geometry). On the other hand, far-wing red-wing excitation preferentially pumps the attractive potential-energy surfaces (e.g., 2B_1 , 2B_2 in C_{2v} geometry or $^2\Pi$ in $C_{\infty v}$ geometry). More accurate modeling of the theoretical difference potentials verify these qualitative considerations. We can thus determine the reaction yield and product state distribution as a function of the electronic symmetry, i.e., as a function of reactant orbital alignment in the complex.

The main results of this work are (a) observation of the the direct reaction of the $\text{Na}^*(4^2P)$ state with H_2 to form NaH and (b) evidence that the reaction proceeds via two

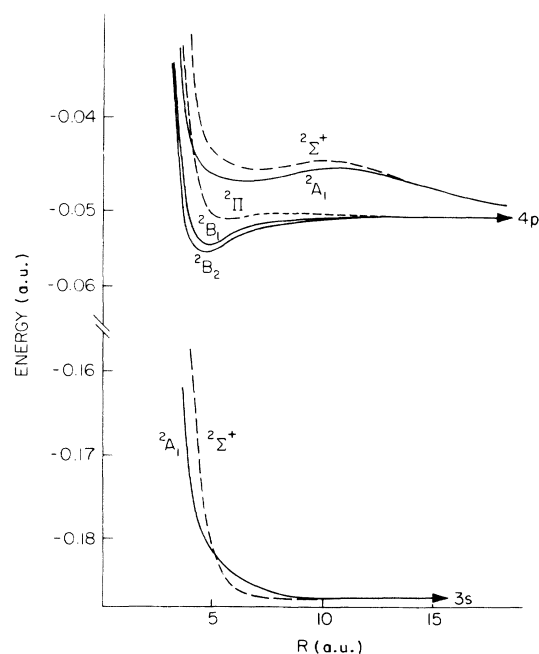


FIG. 1. Potential curves of NaH_2 in C_{2v} (solid lines) and $C_{\infty v}$ (dashed lines) geometry. Taken from Ref. 5.

distinct pathways, one involving the attractive potential surfaces and leading preferentially to high rotational product states, and the other passing over a barrier on the repulsive surface and leading preferentially to low rotational product states.

The details of the experimental pump probe method are similar to that described in Ref. 4. Sodium metal and a hydrogen buffer gas at a typical pressure of 10 Torr are resistively heated in a stainless-steel "cross" oven to a temperature of ~ 670 K corresponding to a sodium density $[\text{Na}] \sim 1 \times 10^{15}/\text{cm}^3$. A frequency doubled and tripled 30-Hz Nd-doped yttrium-aluminum-garnet laser is used to simultaneously pump two tunable pulsed dye lasers in a standard pump probe configuration. The "pump" dye laser is operated near 660 nm and the output is frequency doubled to the spectral region near the $\text{Na}^*(3^2S-4^2P)$ second resonance at 330 nm. The "probe" dye laser is operated in the $A^1\Sigma^+ - X^1\Sigma^+$ band region of NaH near 440 nm. Observation (at right angles to the laser axis) of the $P_{11}(6,1)$ or $P_4(5,1)$ probe-laser-induced fluorescence allows determination of the $v''=1, J''=11$ or 4 populations of the NaH photochemical reaction product. The nonreactive channel is monitored through the collisionally redistributed atomic fluorescence. The emission on the weak $\text{Na}^*(4^2P-3^2S)$ transition is heavily radiatively trapped and quenched leading to weak signals. This problem is exacerbated by the requirement of using narrow spectrometer slits to resolve the resonance fluorescence from the scattered near resonant pump-laser light. For these reasons we have relied on measurements of the cascade fluorescence on the $\text{Na}^*(3^2D-3^2P)$ transition near 820 nm. It should be noted that the D state may also be populated by direct collisional quenching from the $\text{Na}^*(4^2P)$ level. We have not yet made any attempt to distinguish between these two pathways.

The major results of this work are given in Fig. 2. The far-wing profiles show the relative population in the 2(a) $\text{Na}^*(3^2D)$ level (absorption into the nonreactive channel), 2(b) $\text{NaH}(v''=1, J''=4)$ level, and 2(c) $\text{NaH}(v''=1, J''=11)$ level (corresponding to absorption into specific final states of the reactive channels) as a function of pump-laser detuning from the $\text{Na}(3^2S-4^2P)$ resonance line. Due to the different detection schemes the relative normalization between Figs. 2(a) and 2(b), 2(c) is arbitrary. However, Figs. 2(b) and 2(c) are correctly normalized relative to one another. The nonreactive profile 2(a) is quite similar to those obtained using He or Ar as a buffer gas. In particular the pronounced red-wing satellite is also observed in those cases although shifted to smaller detunings. These results will be presented elsewhere. The reactive profiles [2(b) and 2(c)] are very unusual in shape, falling steeply from resonance to a relatively "flat" pedestal. Because this shape is suggestive of some background effect or artifact, we have spent significant effort in verifying the origin of the far-wing signal. Our tests indicate that the reported signals are, in fact, real and associated with the proposed direct reaction process following excitation of the NaH_2 collision complex.

In particular we note that the observed signals are linear in H_2 pressure in the range from ~ 2 to ~ 15 Torr.

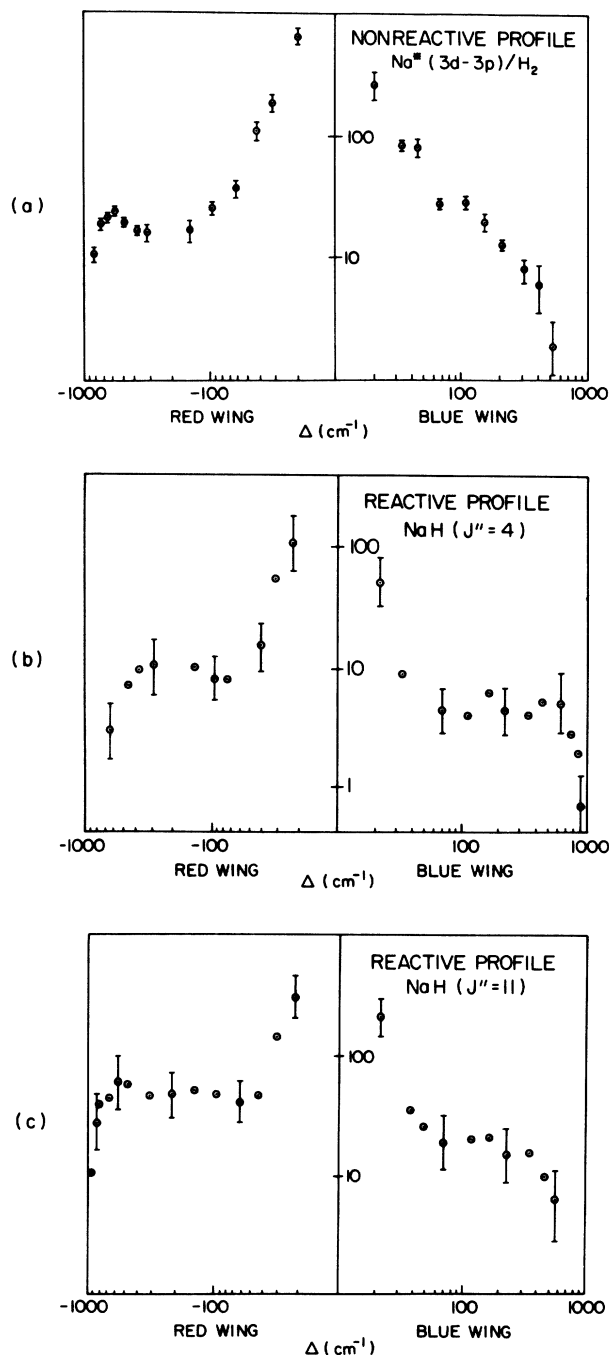


FIG. 2. Excitation profiles of the NaH_2 complex as a function of detuning ($\Delta = \omega_L - \omega_0$) from the $\text{Na}^*(3^2S-4^2P)$ transition: (a) nonreactive profile, $\text{Na}^*(3^2D-3^2P)$ emission; (b) reactive profile, $\text{NaH}(v''=1, J''=4)$ laser-induced fluorescence; (c) reactive profile, $\text{NaH}(v''=1, J''=11)$ laser-induced fluorescence.

They are also independent of pump probe delay time (at a H_2 pressure of 10 Torr), over a range 4–12 ns. These tests effectively rule out multiple collision processes. Measurements at higher pressures do show a contribution from multiple collision processes evidenced by a signal which increases linearly with pump probe delay time. The observed signals are linear in Na density over a range

$\sim 10^{14}$ – $10^{15}/\text{cm}^3$ (600–670 K). Contributions from $\text{Na}_2(\text{C-X})$ dimer absorption in this spectral region have been minimized by taking measurements of the NaH profile at detunings corresponding to minima in the Na_2 absorption band. However, measurements taken at laser wavelengths specifically chosen to excite Na_2 give identical results. These tests conclusively demonstrate that reactions of $\text{Na}_2^*(\text{C}^1\Pi) + \text{H}_2$ are not important under the conditions of this experiment. We will pursue this matter further in future work. The profile measurements were all taken under conditions such that the signals were linear in laser power. Near line center this required the use of neutral density filters to decrease the laser intensity. (At full power, the near line center NaH laser-induced fluorescence (LIF) signals were nonlinear and also showed a linear increase in pump probe delay time indicating the presence of a nonlinear multistep process.) The possible influence of amplified spontaneous emission was ruled out by demonstrating that the observed signals vanish if the dye laser oscillator cavity is spoiled by slightly misaligning the output coupler. Finally, it is important to note that the observed NaH absorption profiles are not completely flat, but in fact fall off dramatically beyond $\sim 700 \text{ cm}^{-1}$ from the $\text{Na}^*(3^2\text{S}-4^2\text{P})$ resonance, as expected and in agreement with the nonreactive $\text{Na}^*(3^2\text{D}-3^2\text{P})$ profile.

Comparison of the reactive and nonreactive profiles in the red and blue wings gives information regarding the overall reactivity on different electronic surfaces (Fig. 3). In the red wing, the NaH:Na * ratio increases with detuning beyond $\sim 50 \text{ cm}^{-1}$ to the kT limit near $\sim 700 \text{ cm}^{-1}$. This steplike behavior in the reactive to nonreactive branching ratio following red-wing excitation was also observed in our previous studies of the $\text{Mg} + \text{H}_2$ reactions.⁴ It may be associated with onset of bound or quasibound absorption in the complex. It might also result from a surface crossing phenomenon.⁶

The reactive to nonreactive branching (NaH:Na *) in the far blue wing increases sharply (perhaps exponentially). We believe this result can be interpreted in terms of reaction over a barrier on the repulsive surface. Such a barrier ($\sim 2000 \text{ cm}^{-1}$) is expected from the pseudopotential

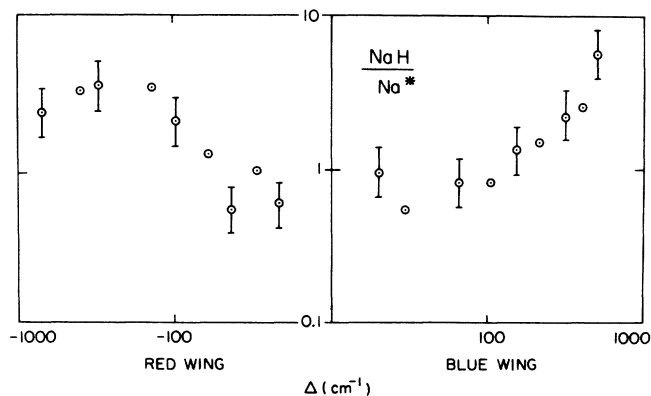


FIG. 3. Reactive to nonreactive branching ratio: i.e., the ratio of the total $\text{NaH}(v''=1, J''=4) + \text{NaH}(v''=1, J''=11)$ LIF signals to the $\text{Na}^*(3^2\text{D}-3^2\text{P})$ emission as a function of detuning. The vertical scale is in relative units only.

calculations of Rossi and Pascale.⁵ For small detunings, only the very-high-energy tail of the Boltzmann distribution has sufficient energy to clear the barrier and the reaction probability is low. As the laser is tuned farther into the blue wing, absorption occurs nearer the top of the barrier and reaction over the barrier becomes possible. The reaction probability is apparently high for trajectories which clear the barrier and the reactive channel dominates. The decreasing reaction probability near line center may be associated with direct "antistatic" wing absorption to the attractive surfaces, or with absorption to the repulsive surfaces followed by rotational coupling to the attractive surfaces. Subsequent reaction may then occur on the attractive surfaces. Both of these processes will decrease rapidly as the blue-wing detuning increases.

Comparison of the branching to different product rotational states is also interesting (Fig. 4). Deep in the red wing, excitation to the attractive surfaces favors the higher rotational state ($J''=11$) over the lower rotational state ($J''=4$). This observation is consistent with a side-on attack mechanism as proposed by Sevin and Chaquin,⁶ and a similar mechanism to explain the reaction of $\text{Mg}^* + \text{H}_2$. Far-blue-wing excitation to the repulsive surfaces favors production of the lower rotational product state ($J''=4$) over the higher state ($J''=11$). This observation is perhaps indicative of an end-on attack mechanism.²

Our results clearly demonstrate the direct reaction of $\text{Na}^*(4^2\text{P}) + \text{H}_2$ can proceed via two distinct pathways: (1) On the attractive surfaces leading preferentially to higher rotational product states, and (2) over a barrier on the repulsive surfaces leading preferentially to lower rotational product states. This remarkable observation is not unique. Similar conclusions^{7,8} have recently been drawn from an investigation of the reaction of $\text{Hg}^*(6^3\text{P})$ with H_2 . Much more work needs to be done to clarify these preliminary results and conclusions.

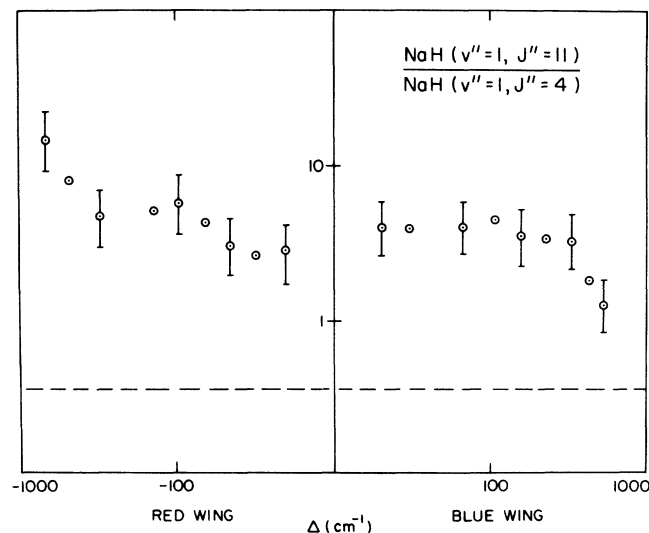


FIG. 4. Branching into different product rotational states; i.e., the ratio of $\text{NaH}(v''=1, J''=11)$ to $\text{NaH}(v''=1, J''=4)$ vs detuning. The vertical scale is in absolute units; the dashed line gives the thermal ratio at 670 K.

We would like to acknowledge helpful discussions with K. M. Sando, W. Kearney, and W. C. Stwalley. This work was supported by the National Science Foundation.

-
- ¹B. Sayer, M. Farray, J. Lozingot, and J. Berlande, *J. Chem. Phys.* **75**, 3894 (1981); J. P. Visticot, M. Farray, J. Lozingot, and B. Sayer, *J. Chem. Phys.* **79**, 2839 (1983).
- ²C. Crepin, J. L. Picque, G. Rahmat, J. Verges, R. Vetter, F. X. Gadea, M. Pelissier, F. Spiegelmann, and J. P. Malrieu, *Chem. Phys. Lett.* **110**, 395 (1984); F. X. Gadea, F. Spiegelmann, M. Pelissier, and J. P. Malrieu, *J. Chem. Phys.* **84**, 4872 (1986); B. Lepetit, M. Le Dourneuf, J. M. Launay, and F. X. Gadea, *Chem. Phys. Lett.* **135**, 377 (1987); B. Lepetit, J. M. Launay, M. Le Dourneuf, and F. X. Gadea, *Chem. Phys.* **117**, 17 (1987).
- ³K. C. Lin and H. C. Chang, *J. Chem. Phys.* **90**, 6151 (1989).
- ⁴P. D. Kleiber, A. M. Lyyra, K. M. Sando, V. Zafropoulos, and W. C. Stwalley, *J. Chem. Phys.* **85**, 5493 (1986).
- ⁵F. Rossi and J. Pascale, *Phys. Rev. A* **32**, 2657 (1985).
- ⁶A. Sevin and P. Chaquin, *J. Chem. Phys.* **93**, 49 (1985).
- ⁷W. H. Breckenridge, C. Jouvet, and B. Soep, *J. Chem. Phys.* **84**, 1443 (1986).
- ⁸O. Nedelec and M. Giroud, *Chem. Phys. Lett.* **165**, 329 (1990).